PCCP

Physical Chemistry Chemical Physics

www.rsc.org/pccp

Volume 14 | Number 18 | 14 May 2012 | Pages 6133–6640

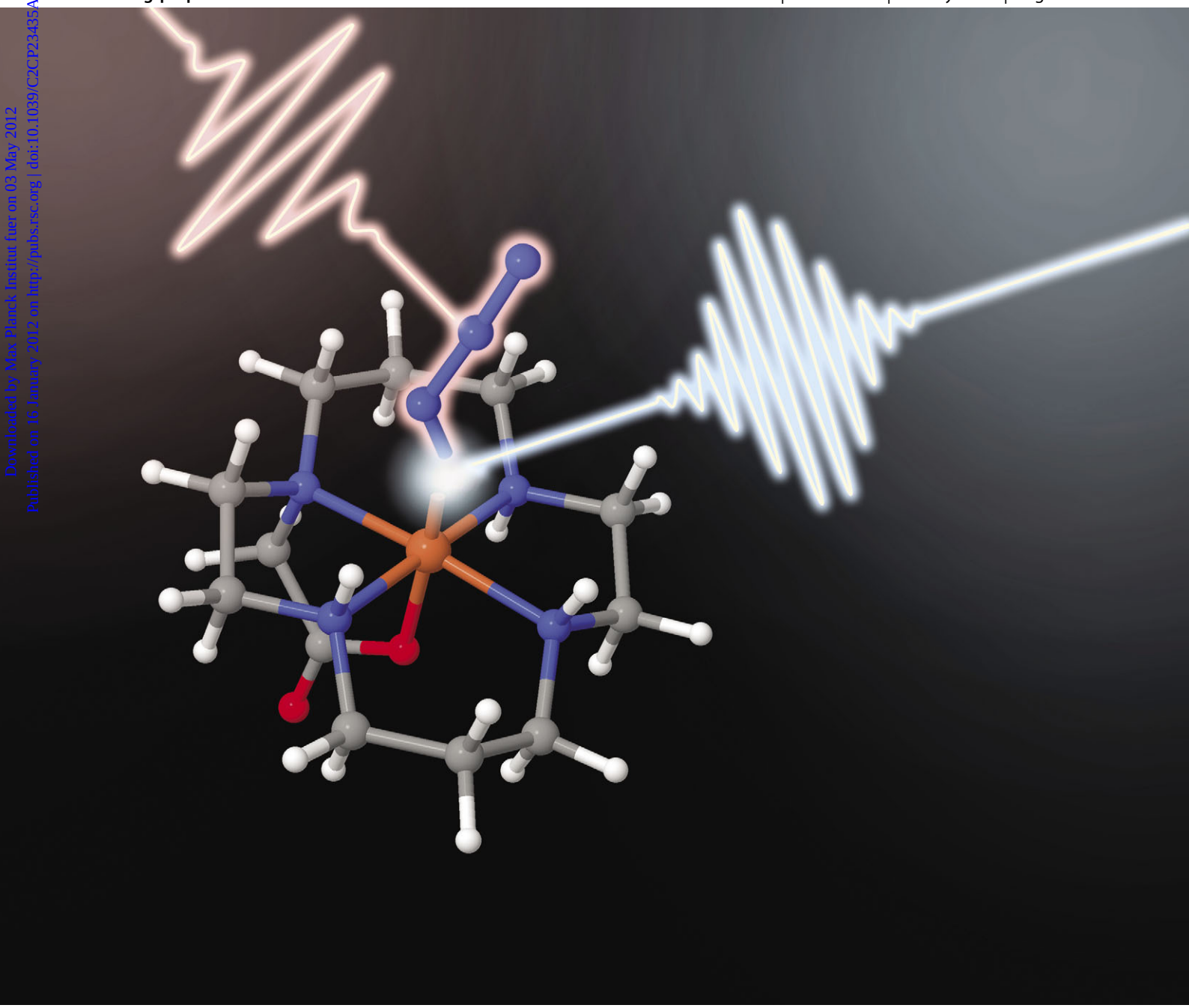

ISSN 1463-9076

COVER ARTICLE

Vöhringer *et al.*

Ultrafast primary processes of an iron-(III) azido complex in solution induced with 266 nm light

PCCP

Dynamic Article Links
View Online

Cite this: *Phys. Chem. Chem. Phys.*, 2012, **14**, 6165–6172

www.rsc.org/pccp

PAPER

Ultrafast primary processes of an iron-(III) azido complex in solution induced with 266 nm light†

Hendrik Vennekate,[a] Dirk Schwarzer,*[a] Joel Torres-Alacan,[b] Oliver Krahe,[bc] Alexander C. Filippou,[c] Frank Neese[b] and Peter Vöhringer*[b]

Received 31st October 2011, Accepted 12th January 2012
DOI: 10.1039/c2cp23435a

The ultrafast photo-induced primary processes of the iron-(III) azido complex, $[Fe^{III}N_3(cyclam\text{-}acetato)]\ PF_6$ (**1**), in acetonitrile solution at room temperature were studied using femtosecond spectroscopy with ultraviolet (UV) excitation and mid-infrared (MIR) detection. Following the absorption of a 266 nm photon, the complex undergoes an internal conversion back to the electronic doublet ground state at a time scale below 2 ps. Subsequently, the electronic ground state vibrationally cools with a characteristic time constant of 13 ps. A homolytic bond cleavage was also observed by the appearance of ground state azide radicals, which were identified by their asymmetric stretching vibration at 1659 cm^{-1}. The azide radical recombines in a geminate fashion with the iron containing fragment within 20 ps. The cage escape leading to well separated fragments after homolytic Fe–N bond breakage was found to occur with a quantum yield of 35%. Finally, non-geminate recombination at nanosecond time scales was seen to further reduce the photolytic quantum yield to below 20% at a wavelength of 266 nm.

I. Introduction

Remarkable research efforts of the bioinorganic and coordination chemistry communities are directed toward the synthetic preparation of metal centers at unusually high oxidation states because of their possible involvement in the catalytic cycles of a variety of heme and non-heme metalloproteins.[1–4] The most prominent example is the enzymatic oxidation for which nature has evolved the cytochrome P450 superfamily of enzymes.[5] These proteins carry an iron-coordinating protoporphyrin-IX prosthetic group as the active site where a transient ferryl-oxo species of the type Fe(IV)=O is able to catalyze the hydroxylation of a substrate by an "oxygen rebound" mechanism.[6] While quantum chemical methods have been highly instrumental in characterizing the electronic structure of such "high-valent" iron centers,[7–9] the collection of hard spectroscopic evidence for their existence during the sequence of biochemical transformations proves to be a demanding but inevitable challenge.

The creation of *in vitro* precedents for high-oxidation state iron compounds requires pursuing a twofold strategy. Firstly, efficient synthetic pathways need to be devised that can carry—if possible, quantitatively—the metal center to the desired high oxidation state and secondly, suitable artificial molecular coordination environments have to be designed that can stabilize these highly electron deficient metal configurations. The stabilization is required to last for a sufficiently long period to facilitate an experimental verification of the metal center in the high oxidation state, presumably by spectroscopic means such as electron paramagnetic resonance (EPR) or Mössbauer spectroscopy.

Inspired by early work on the preparation of chromium(V) and manganese(V) porphyrins bearing a nitrido ligand,[10,11] Wagner and Nakamoto were able to generate a corresponding nitridoiron(V) complex through laser irradiation of a azidoiron(III)-porphyrin precursor complex and to identify the nitrido complex by its Fe–N stretching vibration in resonance-Raman spectroscopy.[12] Based on these efforts, Wieghardt and coworkers developed a synthetic pathway towards high oxidation state iron, which also relied on the photochemical decomposition of an azido-complex carrying an iron center at a lower oxidation state.[13–16] However, rather than stabilizing the "high-valent" state through a biomimetic porphyrin scaffold, the metal center was embedded into the environment provided by the pentadentate ligand, 1,4,8,11-tetraazacyclotetradecane-1-acetate, hereafter referred to as the cyclam-acetato moiety (see Scheme 1).

Whether the precursor is photo-reduced or—as is desired—photo-oxidized depends sensitively on the choice of the photolysis wavelength. Homolytic Fe–N cleavage delivers the next lower valent metal center and an azide radical as the primary dissociation products, of which the latter subsequently evolves into dinitrogen.

[a] *AG Reaktionsdynamik, Max-Planck-Institut für biophysikalische Chemie, Am Faßberg 11, 37077 Göttingen, Germany. E-mail: dschwar@gwdg.de*
[b] *Institut für Physikalische und Theoretische Chemie, Rheinische Friedrich-Wilhelm-Universität, Wegelerstraße 12, 53115 Bonn, Germany. E-mail: p.voehringer@uni-bonn.de*
[c] *Institut für Anorganische Chemie, Rheinische Friedrich-Wilhelms-Universität, Gerhard-Domagk-Straße 1, 53121 Bonn, Germany*
† Electronic supplementary information (ESI) available. See DOI: 10.1039/c2cp23435a

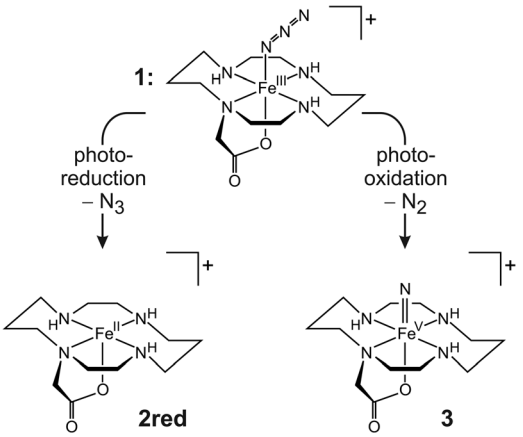

Scheme 1 Photochemical pathways of the (cyclam-ac)-azido-iron(III) complex **1**.

The alternative pathway includes the preferred N–N bond fission and generates a terminal nitrido ligand while formally the metal center is oxidized by two units. In particular, Grapperhaus *et al.* irradiated the azido complex, $[Fe^{III}N_3(cyclam\text{-}ac)]PF_6$ (**1**), which has a low-spin (d^5, $S = 1/2$) doublet ground state, in frozen and liquid acetonitrile solutions with light of various wavelengths.[14]

Irradiation of **1** at 300 nm in acetonitrile at room temperature[14] resulted in photo-reduction and yielded predominantly the Fe^{II} complex, **2red**, which is a low-spin (d^6, $S = 0$, singlet) iron(II) complex that coordinates a solvent molecule at the vacant axial position. The existence of a minor photo-oxidation pathway at a photolysis wavelength of 300 nm was deduced indirectly by the formation of a binuclear mixed-valence adduct complex carrying most likely an iron(IV)-site at low temperature. While excitation at around 300 nm favored the photo-reduction channel, an irradiation of compound **1** in acetonitrile with 420 nm light at 80 K generated the desired iron(V)nitrido complex, **3**, in high yields.[14] X-Ray absorption and Mössbauer spectroscopy as well as magnetic measurements have later revealed that the Fe(V) complex exhibits a doublet ground state and not a quartet, as initially assumed.[17] Fascinatingly, when the cyclam-ac ligand was N-methylated, the corresponding iron(III)azido complex could also be oxidized electrochemically thereby affording an iron(IV) complex (d^4, $S = 1$, triplet),[13] which subsequently served as a photochemical precursor to an octahedral iron(VI) complex featuring a low-spin singlet ground state (d^2).[16]

Despite these impressive synthetic and analytical research efforts on this important class of compounds, practically nothing is known with respect to their photo-induced elementary dynamics and relaxation mechanisms. This paper intends to fill this gap by reporting on the real-time observation of the molecular dynamical processes that are triggered by absorption of an ultraviolet (UV) photon by the iron(III) azido complex, **1**. In contrast to the previous studies reported so far, we focus on the molecular reaction dynamics rather than the steady-state photochemistry of **1** in liquid acetonitrile solution at room temperature. Because of the ultrafast nature of the light-induced primary processes of transition metal complexes in liquid solution, femtosecond spectroscopy was carried out. More specifically, a detection in the mid-infrared (mid-IR) spectral region was employed that is particularly sensitive to the acetato-CO and N_3-stretching vibrations of the parent metal complex and the putative reaction products of the primary photo-induced processes. We focus further on the elementary dynamics that are induced by femtosecond pulses having a wavelength of 266 nm, *i.e.* with light that leads primarily to the photo-reduction of the precursor complex. This will set the stage for a forthcoming publication devoted to unraveling the dependence of the ultrafast photochemistry of **1** on the excitation wavelength including the photo-oxidation pathway. The mechanistic insights into the photochemistry of such metal complexes obtained from ultrafast spectroscopic experiments might provide useful guidelines in the future for bioinorganic chemists in their quest of designing novel and efficient synthetic routes to high-oxidation state iron centers.

II. Methods

UV-pump–IR-probe experiments were performed with a laser system based on a 1 kHz Ti : sapphire oscillator/regenerative amplifier producing 150 fs pulses at 800 nm with pulse energies of 0.7 mJ. The excitation wavelength of 267 nm was produced by third harmonic generation of a small portion of the 800 nm regenerative amplifier output. Pump pulse energies entering the sample were 1–2 μJ. The spot size of the pump radiation inside the sample was about 200 microns in diameter thereby resulting in excitation power densities of around 30 GW cm^{-2}. Tunable mid-infrared probe pulses were generated by difference frequency mixing of signal and idler pulses from an optical parametric amplifier pumped by half of the regenerative amplifier energy. The IR pulses were split into a probe and a reference beam. The latter was superimposed on the pump beam and both were focused into the sample cell. The spot size of the probe radiation was slightly below the pump diameter, *i.e.* 180 microns. The relative plane of polarization was set to 54.7°. Behind the sample the reference and probe beam were directed to a polychromator and their spectra were imaged on a liquid-nitrogen cooled HgCdTe detector of 2 × 32 pixels. To avoid spectral and temporal distortion of the IR pulses by CO_2 and water absorptions in air, the whole pump–probe setup was purged with dry nitrogen.

The experiments were performed with 1 mM solutions of compound **1** in acetonitrile-d_3 in a stainless steel flow cell with CaF_2 windows of 1 mm thickness. The optical path length inside the cell was 0.6 mm and the transmission at the pump wavelength was 10–20%. The solvent acetonitrile-d_3 (99.5% deuteration) was purchased from Deutero. The synthesis of complex **1** as described in ref. 14 was slightly modified to provide larger quantities necessary for successfully conducting the pump–probe spectroscopy. Details of the synthesis are presented elsewhere and in the ESI.†[18]

All quantum chemical calculations were carried out with the ORCA electronic structure program.[19] Structures were optimized with the B3LYP density functional[20,21] in conjunction with the RIJCOSX approximation.[22] In all calculations, the def2-TZVP basis was used together with the appropriate auxiliary basis set required for invoking the RI approximation.[23,24] For increased accuracy, 10^{-9} Eh was used as convergence criteria for the energy change in the SCF procedure and the size of the DFT integration grid was increased to 434 points (the default value is 110 for the scf procedure and 302 for the final calculation).

Molecular structures were considered to be converged in the optimization when the root mean square (RMS) of the gradient is below 3×10^{-5} Eh bohr^{-1}, the RMS of the displacements is below 6×10^{-4} bohr and the energy change compared to the previous optimization step is below 10^{-6} Eh. Vibrational frequency calculations were performed through two-sided numerical differentiation of the analytical gradient. $6N$ displacements were calculated (N is the number of atoms) with a numerical increment of 0.005 bohr. All structures were verified to represent true local minima on the potential energy surface. In order to compare the calculated harmonic frequencies with experimental fundamentals a scaling factor was used. For the B3LYP functional used here, the scaling factor is 0.9614, which is very close to unity. A calibration study has shown that the root mean square deviation for the deviation between experimental and calculated frequencies with this setup is $\sim$34 cm^{-1}.[25] Solvent effects were taken into account in terms of the conductor like screening model (COSMO).[26,27] To compare the energetic preference of an assumed intermediate, complete active space self-consistent field calculations (CASSCF) were performed. We did this in a state average manner over the first 10 roots. The CASSCF wave function was further used for N-valence perturbation theory (NEVPT2) calculations to cover effects of dynamic correlation. In both cases the chosen active space consists of the five iron d-orbitals as well as a doubly occupied π-bonding and a vacant π-anti-bonding orbital of the azide ligand. DFT orbitals from above were used as a guess for the CASSCF/NEVPT2 procedure.

III. Results and discussion

1. Linear spectroscopy

The electronic absorption spectrum in the ultraviolet and visible spectral region of **1** in acetonitrile at 298 K is displayed in Fig. 1. It basically consists of two spectroscopically distinct absorption profiles. The first of which peaks at 455 nm, *i.e.* in the near-UV-to-visible region, and is rather weak ($\sim$2000 M^{-1} cm^{-1}). Its low-energy tail extends well beyond 600 nm thereby giving this crystalline compound its characteristic orange-brown color. This resonance has previously been attributed to a ligand-to-metal charge-transfer (LMCT) state,[17] whose excitation results in a cleavage of the azido ligand's N–N bond concomitant with the direct formation of di-nitrogen and the desired high-valent iron(v)-nitrido species **3** (see Scheme 1).

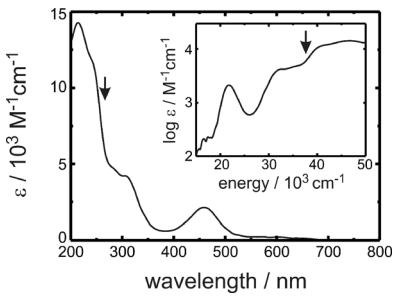

Fig. 1 UV/Vis absorption spectrum of the (cyclam-ac)-azidoiron(III) complex **1** in liquid acetonitrile solution under ambient conditions. The vertical arrow indicates the spectral position of the excitation pulses.

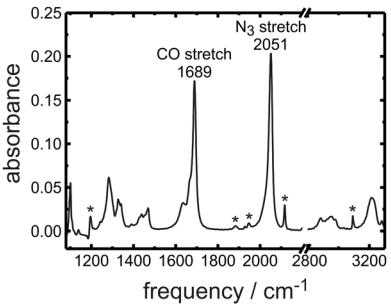

Fig. 2 FTIR spectrum of the (cyclam-ac)-azidoiron(III) cation complex **1** in liquid acetonitrile solution under ambient conditions. The asterisks mark absorption bands of the solvent.

The second absorption profile extends deep into the ultraviolet spectral region and displays characteristic absorption maxima (at 305 and 215 nm) and shoulders (at 275 nm and 240 nm). Although the exact nature of these spectral features has been entirely unknown so far, irradiation at such low wavelengths was reported to result in a homolytic cleavage of the Fe–N bond thereby transiently forming an azide radical and an iron(II) complex that is stabilized by the attachment of an acetonitrile solvent molecule.[14] Since the electronic ground state of **1** is a low-spin doublet state, D_0, we will tentatively denote the higher lying electronic states that give rise to the resonances below 360 nm as $D_{2,3}$ while the LMCT state is D_1. The pump–probe experiments reported herein have been conducted with pump pulses centered at 266 nm thereby exclusively exciting the absorption region associated with photo-reduction.

A Fourier-transform infrared (FTIR) spectrum of the parent complex **1** dissolved in liquid deuterated acetonitrile at room temperature is displayed in Fig. 2. It features two highly characteristic vibrational bands in the mid-IR spectral region. The carboxylate stretching vibration of the cyclam-acetato ligand is located at 1689 cm^{-1}, while the stretching vibration of the azido ligand can be found at 2051 cm^{-1}. This assignment is further substantiated by quantum chemical calculations on iron(III)-complex **1** based on density functional theory, which provides scaled harmonic frequencies of 1715 cm^{-1} and 2078 cm^{-1} for the CO and N_3 stretching modes.

The deuterated solvent provides ample transmission in the frequency region between 1200 cm^{-1} and 2200 cm^{-1} and the primary processes that result from an ultrafast electronic excitation of the parent complex should therefore be observable in this frequency region. Firstly, a bond cleavage either within the ligand or between the ligand and the metal center can be expected to modify the electronic charge-distribution among the atoms of the complex. As a result, the carboxylate vibrational resonance of the iron containing fragment should be spectrally shifted from the corresponding CO-stretching vibration of the iron complex in its electronic ground state. The same holds true—although to a lesser extent—for the carboxylate and azido stretching modes of the higher lying electronic states of parent compound **1** that are accessed either directly by the pump pulse or possibly transiently *via* non-adiabatic transitions prior to dissociation. Furthermore, the anti-symmetric stretching vibration of a putative azide radical product is expected to differ from the stretching vibrations of the azido ligand attached to the iron center. Hence, the photo-reduction should also result

in changes of the vibrational spectrum in the azido stretching region. Finally, one should stress that an N–N bond cleavage within the azido ligand produces a diatomic fragment (dinitrogen) that is IR silent. As a result, the photo-oxidation pathway although not necessarily implicated in the 266 nm photolysis of **1** may not be as straightforwardly detected in time-resolved infrared experiments such as those reported here.

2. Femtosecond spectroscopy

Irradiation of the iron(III) complex with femtosecond pulses centered at 266 nm results in a spectro-temporal response in the parent acetato-CO stretching region that is displayed in Fig. 3. At the earliest delay (440 fs), the pump-induced (or differential) optical density, ΔOD, displays a negative band at a frequency of exactly 1689 cm^{-1} corresponding to spectral position of the stationary acetato-CO stretching absorption of **1** in its electronic ground state. A negative differential optical density indicates an increased optical transmission of the sample relative to its linear stationary transmission as a result of the excitation with the 266 nm pulse. An increased transmission arises because the photolysis pulse has removed molecules of **1** from their electronic ground state and promoted them to the electronically excited state. Therefore, the sample is said to be bleached by the pump-pulse at the frequency where the electronic ground-state absorbs.

Apart from this so-called ground-state bleach, a positive band can also be observed in Fig. 3, which peaks at 1650 cm^{-1}, *i.e.* shifted to lower frequency as compared to the stationary parent CO stretching absorption. A positive pump-induced optical density indicates a decreased optical transmission relative to the stationary transmission, which can only occur if new absorber species are created by the photolysis pulse whose absorption spectra are distinct from that of parent compound **1** in its electronic ground state. The most obvious absorber that is newly created by the ultraviolet excitation is the dipole-allowed electronically excited state of parent complex, *i.e.* **1*** or more precisely, the $D_{2,3}$ of **1**, that is accessed by the 266 nm photolysis photon. Apparently, the carboxylate group of **1*** experiences a slightly higher electron density in comparison to **1** thereby exhibiting a slightly decreased stretching frequency relative to the electronic ground state.

As the time delay is increased, the parent CO bleach partially recovers indicating that a significant fraction of the iron complexes return to their electronic ground state. Concurrently, the induced absorption also decays but to a much smaller extent as judged from the band peak intensities. While the parent CO bleach has recovered within the first 80 ps by about 60%, the excited state absorption has decayed during the same time by ~30% only. Furthermore, an isosbestic probe frequency at which the pump-induced optical density remains delay-independent is clearly not observed. Rather, the complex spectro-temporal evolution between induced bleach and induced absorption suggests that the thermalized electronic ground state of the iron complex is not directly replenished by the decay of the dipole-allowed excited state, **1***, that is initially prepared by the pump pulse. For example, intermediate electronic states whose CO stretching frequency or CO transition dipole moment differ from those of the parent ground state may become transiently populated. Alternatively, upon its recovery the ground electronic state may be vibrationally excited either directly in the carboxylate mode or in other vibrational modes to which the CO stretch is anharmonically coupled. Furthermore, a bond dissociation followed by a geminate (*i.e.* in-cage) recombination of the fragments might precede the refilling of the ground electronic state of **1** thereby further complicating the spectro-temporal evolution in the mid-infrared spectral region by virtue of the fragment's own IR active vibrational modes.

A closer inspection of the spectral shape of the induced absorption at late delays reveals (i) the existence of a pronounced shoulder at a frequency of 1640 cm^{-1} and (ii) a slight dynamic shift of the peak position from 1650 cm^{-1} to 1655 cm^{-1} as the time delay is increased. While the latter finding may be tentatively rationalized with vibrational cooling and/or solvation dynamics of the $D_{2,3}$ excited state, the low-frequency shoulder strongly suggests that the induced absorption is actually composed of two vibrational bands rather than one. To follow up on this notion, the pure absorptive component of the long-time transient spectrum (*i.e.* 80 ps after photolysis) is extracted by adding the appropriately scaled linear FTIR spectrum of the parent complex so as to fully remove the perturbing ground-state bleach.

The resulting difference spectrum is displayed in Fig. 4 (symbols) and compared to a spectral fit composed of two Gaussian line shapes of the form

$$\Delta\mathrm{OD}(\tilde{\nu}) = A \exp\left[-4 \ln 2 \left(\frac{\tilde{\nu} - \tilde{\nu}_0}{\sigma}\right)\right]. \qquad (1)$$

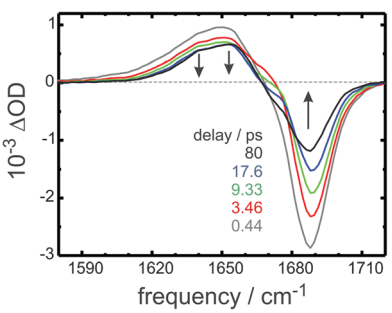

Fig. 3 Femtosecond pump–probe spectra in the acetato-CO region following 266 nm optical excitation of the (cyclam-ac)-azidoiron(III) cation complex **1** in liquid acetonitrile solution under ambient conditions. The vertical arrows emphasize the principal spectral components.

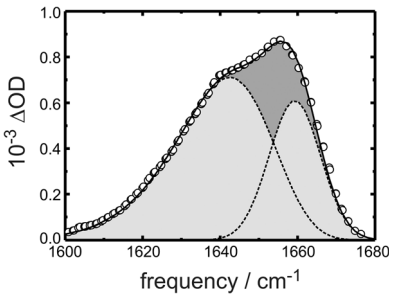

Fig. 4 Experimental difference spectrum (symbols) obtained by subtracting the scaled FTIR-experiment from the femtosecond pump–probe spectrum recorded at a delay of 80 ps. The solid curve is a fit to the data using a superposition of two Gaussian components (dashed curves). For details see the text.

One of the two Gaussian components has a central frequency, $\tilde{\nu}_0$, of 1659 cm^{-1} and a full width at half maximum, σ, of 16 cm^{-1}. The second component with a relative amplitude of 0.54 and a central frequency of 1643 cm^{-1} is skewed asymmetrically to lower frequencies using a frequency-dependent width, $\sigma = \sigma(\tilde{\nu}) = 2\sigma_0/\{1 + \exp[a(\tilde{\nu} - \tilde{\nu}_0)]\}$, with an asymmetry parameter, a, of 0.017 and a center width, σ_0, of 29 cm^{-1}.

The existence of two distinct vibrational resonances in the acetato-CO stretching region at later delay times can be explained by the photo-induced Fe–N bond cleavage that was already concluded by Wieghardt and coworkers[14] from their steady-state irradiation experiments on compound **1** in room temperature acetonitrile solutions using 300 nm light. In these previous studies, the homolytic character of the photo-dissociation was deduced indirectly using a combination of electronic absorption and Mössbauer spectroscopy on the accumulated low-spin iron(II) photoproduct complex **2red**. However, an observation of the nitrogen-carrying fragment, *i.e.* the azide radical, would constitute a more direct piece of evidence for the homolytic mechanism of photo-dissociation. Unfortunately, due to its very short lifetime in liquid solution, the azide radical fragment of the photo-reduction could not be detected in such steady-state experiments.

So far, azide radicals in liquid solution have only been detected by electronic absorption spectroscopy where it features a characteristic UV resonance at 277 nm.[28,29] To our knowledge, the vibrational spectra of $N_3^{\bullet}$ in the liquid phase have not yet been recorded. However, the asymmetric stretching fundamental of $N_3^{\bullet}$ in the gas phase has been located at 1645 cm^{-1} using FTIR absorption spectroscopy.[30] Furthermore, the same vibration was seen to absorb at 1658 cm^{-1} when $N_3^{\bullet}$ was prepared in a solid N_2 matrix at 20 K.[31] In light of these gas and solid phase data, it seems highly probable that the absorptive 1659 cm^{-1} component in the transient spectrum of the parent complex seen at 80 ps after photolysis is indeed brought about by the azide radical. From this comparison, one would then continue to conclude that the low-frequency component peaking in Fig. 4 at 1643 cm^{-1} originates from the acetato-CO-vibration of the second metal-containing fragment, **2red** or electronically excited configurations thereof, as well as from the excited state, **1***, of the parent complex. This is in reasonable agreement with our frequency calculations based on DFT, which identify carbonyl stretching vibration of **2red** at 1689 cm^{-1} and the asymmetric stretching vibration of $N_3^{\bullet}$ at 1643 cm^{-1}.

The question arises as to how and when the linear azide radical is actually formed once the parent complex has absorbed a 266 nm photon. This question cannot be easily answered from the pump–probe data shown in Fig. 3 because of the strong spectral overlap of the multiple components, *i.e.* the asymmetric stretch of the azide radical and the acetato-CO stretch of the parent ground and excited states as well as of the metal containing the fragment (*cf.* Fig. 4). Further information for addressing these issues might be obtained from femtosecond photolysis experiments by probing in the asymmetric stretching spectral region of the azido ligand at around 2050 cm^{-1}. Corresponding pump–probe spectra are shown in Fig. 5 for a few representative time delays after the initial 266 nm photolysis.

It can be seen that immediately after excitation (*i.e.* at a delay of 0.38 ps) the azido stretching band of the parent

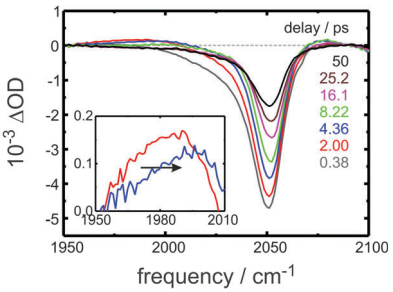

Fig. 5 Femtosecond pump–probe spectra in the azido stretching region following 266 nm optical excitation of the (cyclam-ac)-azidoiron(III) cation complex **1** in liquid acetonitrile solution under ambient conditions. The vertical arrows emphasize the principal spectral components.

complex **1** is bleached because its ground electronic state is depopulated by the photolysis pulse. We would have anticipated observing some spectral signature of the optically accessed excited electronic state of complex **1** however; at such early delays no spectrally nearby induced absorption is detected that is about as intense as the ground-state hole. The lack of an excited-state signature in the azido stretching region can in principle be interpreted by a breakage of the Fe–N bond that occurs faster than the time-resolution of our experimental apparatus. However, as alluded to above, a closer inspection of the acetato-CO region reveals some considerable shifting of spectral amplitude within the first hundred picoseconds, which indicates that the formation of the thermalized azide radical may not be such a prompt process.

Following quantum chemical calculations,[32–35] the N_3 molecule in its electronic ground state, $\tilde{X}^2\Pi_g$, is linear and in this geometry, the first excited state is $\tilde{A}\,^2\Sigma_g^+$ corresponding to a single excitation of $\tilde{X}^2\Pi_g$. The next lowest excited state in $D_{\infty h}$ is the doubly degenerate, $\tilde{B}^2\Pi_u$ state, which splits into two components, $^2B_1$ and $^2A_1$, upon lowering the symmetry to C_{2v}. In the gas phase, the $^2B_1$ component becomes the lowest lying bound excited state when the geometry is fully relaxed to form an acute isosceles triangle. Owing to large energy barriers in excess of 30 kcal mol^{-1}, this cyclic-N_3 is stable against both, linearization back to the ground state and dissociation into N_2 and a nitrogen atom.[33,35]

From these energetics, it is in principle possible that the azide radicals are transiently trapped as a cyclic isomer when complex **1** is excited with 266 nm light. Complete active space self-consistent field (CASSCF) calculations[32] employing the full valence space, CAS(15,12), and Dunning's augmented cc-pVTZ basis set provide a harmonic anti-symmetric stretching frequency of 1659 cm^{-1} for the linear azide radical, *i.e.* in quantitative agreement with our experiment (see Fig. 4). The same level of theory locates the symmetric breathing mode of the cyclic-N_3 at a harmonic frequency of 1632 cm^{-1}, *i.e.* also slightly down-shifted in comparison to the acetato-CO-mode of compound **1**. However, for symmetry reasons the infrared activity of this mode turns out to be almost two orders of magnitude weaker than that of the asymmetric stretch of the linear radical. This makes it practically impossible to detect the cyclic N_3 isomer in a time-resolved infrared experiment such as ours. If indeed the azide radical is initially formed as a cyclic isomer within the time-resolution of the experiment,

there will be neither a spectroscopic fingerprint of the electronically excited state in the N_3 stretching region nor of the azide radical in the acetato-CO region at early delays. Both conclusions would in principle be consistent with the experimental data shown in Fig. 3 and 5, however an unambiguous detection of an azide radical that is possibly trapped as a cyclic intermediate can only be achieved by time-resolved Raman spectroscopy.

Referring again to Fig. 5, the azido bleach clearly recovers as the time delay increases indicating the return of a fraction of photo-excited complexes to their electronic ground state. This observation is consistent with the bleach recovery seen in the acetato-CO stretching region (*cf*. Fig. 3). Simultaneously, an extremely weak and broad induced absorption appears within 2 ps that is considerably red-shifted as compared to the ground-state bleach. With further increasing time delay, this subtle feature gradually decays while continuously shifting to higher frequencies.

It is possible to calculate the time-dependent absorption spectrum in the azido stretching spectral region of those iron complexes that were initially photo-excited and refill the ground electronic state of **1** either through geminate recombination of the fragments following an initial bond dissociation or simply *via* internal conversion without ever forming fragments at all. To this end, the early time pump–probe spectrum (*i.e*. at 0.38 ps) is subtracted for each time delay from the frequency-dependent pump-induced optical densities. Such pump-induced difference spectra are shown in Fig. 6 for various delays.

At short times after photolysis, it is evident that in comparison to the corresponding linear absorption, the azido-stretching band of the replenished ground-state complex **1** is substantially downshifted in frequency and is also spectrally extremely broad. As the time delay is increased the absorption band narrows and its peak frequency asymptotically approaches the azido stretching fundamental. Both observations are highly indicative of vibrational relaxation dynamics of the reformed parent complex. Because of the anharmonic character of the vibrational motion, hot transitions within the azido stretching manifold are shifted to lower frequencies as compared to the fundamental. Furthermore, anharmonic couplings to other vibrational modes of the polyatomic complex spectrally congest the fundamental and the hot azido stretching transitions thereby giving rise to the enormous spectral width at early times. As vibrational energy is redistributed among all vibrational modes and excess energy is transferred into the solvent, a room temperature canonical energy distribution is established causing

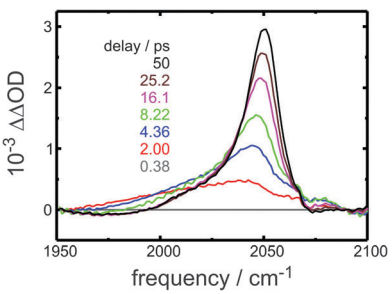

Fig. 6 Femtosecond absorption spectra in the azido stretching region of the replenished electronic ground state of the iron complex **1**. For details see the text.

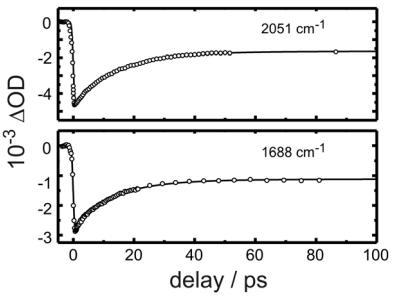

Fig. 7 Femtosecond kinetic traces in the azido stretching region (upper panel) and the acetato-CO region (lower panel) following 266 nm excitation of the iron complex **1** under ambient conditions. The solid curves are fits to multi-exponential decays.

the metal complex to vibrationally "cool". The dynamics of both, intramolecular vibrational redistribution and intermolecular vibrational energy transfer, are reflected in the time-dependent spectral sharpening and upshifting of the azido-stretching absorption band.

To quantify the dynamics of vibrational relaxation, the pump-induced optical density at the frequency of maximal bleaching amplitude (*i.e*. at 2051 cm^{-1}) is plotted as a function of time delay in Fig. 7 (upper panel). Around $t = 0$ the data exhibit an initial instrument-limited drop of the differential optical density, which is due to the interaction of the sample with the photolysis pulse and the concomitant depletion of the electronic ground-state. The bleach partially recovers at a time scale of 100 ps as was already evident from the series of pump–probe spectra shown in Fig. 5. The kinetic trace can be fitted phenomenologically by a bi-exponential decay to which a static offset is added (solid curve). The fitting function was convoluted with a Gaussian temporal profile with a full width at half maximum of 500 fs to take the finite time-resolution of the experiment into account. The dominant exponential has a relative amplitude of 60% with a time constant of 14 ps. A minor exponential accounting for 6% of the total recovery is responsible for an initial ultrafast component with a time constant of 1.5 ps. The remaining 34% static offset represents the finite fraction of complexes that suffers from photochemistry (presumably photo-dissociation under formation of azide radicals) and that does not return to the electronic ground state by geminate recombination.

For comparative purposes, Fig. 7 (lower panel) also displays a kinetic trace recorded at the maximal acetato-CO stretching bleach at 1688 cm^{-1} together with the fit. Again, the overall decay is governed by an exponential with a time constant of 13 ps and a relative amplitude of 53%, while an additional ultrafast component having an amplitude of 11% and a time constant of 1.5 ps contributes to the total decay at early times. Again, a static offset with a relative amplitude of 36% is required to reproduce the long-time tail of the trace that indicates a finite cage escape probability of the photochemical products.

From this analysis we can conclude that within the accuracy of the experiment, the kinetic traces tracking the two bleaching maxima (*i.e*. the azido stretch at 2051 cm^{-1} and the acetato-CO stretch at 1688 cm^{-1}) basically report on the very same dynamical process. From the dynamically evolving spectral shapes we conclude further that these dynamics are essentially the vibrational relaxation dynamics occurring in the ground

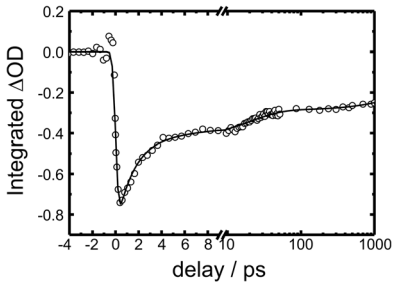

Fig. 8 Temporal evolution of the frequency-integrated azido stretching band following 266 nm excitation of the iron complex **1** under ambient conditions. The solid curve is a fit to a multi-exponential decay. Note the break in the delay axis, which is linear at time shorter than 10 ps and logarithmic elsewhere.

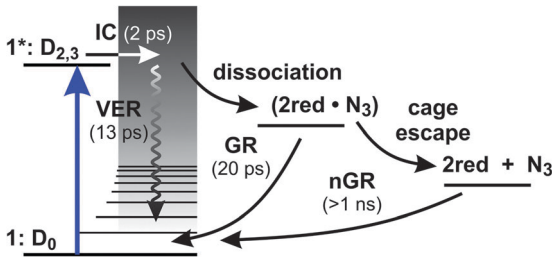

Fig. 9 Sequence of primary photoinduced processes following 266 nm excitation of the iron complex **1** under ambient conditions. The numbers in parentheses indicate the characteristic times of each process. IC = internal conversion, GR = geminate recombination, nGR = non-geminate recombination, VER = vibrational energy relaxation.

electronic state of compound **1** following its ultrafast 266 nm photo-excitation. Vibrational relaxation occurs with a characteristic time constant of 13 ps, which is not unusual for such processes in polyatomic molecules dissolved in dipolar liquids.

To retrieve in a second step the pure electronic population dynamics (as opposed to the vibrational population dynamics in the electronic ground state), the dynamically evolving transient spectrum in the azido stretching region can be integrated over the probe frequency. Provided the N_3-stretching transition dipole moment is independent of the internal energy of the transition metal complex, this band integral is then a measure of the total number density of molecules of **1** residing in their electronic ground state as a function of the pump–probe time delay. Such a trace is depicted in Fig. 8, where the experimental data have again been fitted by a multi-exponential decay. Again, the pump-pulse limited depletion of the ground electronic state is seen around time zero, which is followed by a dynamic refilling that appears to be much faster than the bleach recoveries of the kinetic traces just discussed.

Indeed, the fitting procedure returns a dominant exponential with a relative amplitude of 50% that is ultrafast in nature with a time constant of 1.5 ps. It is evident that this component corresponds to the minor ultrafast contribution seen in the bleach recoveries of Fig. 7. Another second component has a time constant of 20 ps with an amplitude of 18%. The remaining 32% account for the long-time tail, which when measured over delays in excess of 1 ns is clearly seen to continue to decay.

Apparently, the electronic ground state is mostly replenished at a time scale well below 5 ps and we attribute this ultrafast portion to a fraction of complexes returning *via* internal conversion without having suffered from a homolytic bond breakage. This fraction of ground state molecules goes on to vibrationally relax on D_0 at a time scale of 13 ps. In contrast, the 20 ps exponential is then assigned to another fraction of ground-state complexes being reformed after homolytic bond breakage and in-cage recombination of the geminate pairs consisting of an azide radical and an iron-containing cyclam-acetato fragment. Finally, the non-geminate recombination is then made responsible for the ground-state refilling seen in Fig. 8 on nanosecond time scales. Such a process requires the geminate pairs to escape and to separate from their mutual solvent cage. Once drifted into the bulk the fragments can diffusively encounter independent recombination partners that do not originate from the same parent complex. The hierarchy of elementary processes that follow a 266 nm photo-excitation of the iron-complex **1** is schematically sketched in Fig. 9.

What remains unclear at this stage is whether the iron–nitrogen bond is cleaved from a fraction of photo-excited parent molecules directly in their $D_{2,3}$ state (*i.e.* prior to internal conversion) or is cleaved indirectly succeeding the non-adiabatic transition (*i.e.* from energetically high lying vibrational quanta of the D_0 electronic state in competition with vibrational energy relaxation). Finally, we discuss the nature of the internal conversion funneling the molecules back into the ground state but in a vibrationally highly excited manner. We have discussed above that it is at least energetically tenable that the azide radical is initially formed in a bent configuration. It could also well be that the nuclear motions driving the system toward a conical intersection between the $D_{2,3}$ excited and the D_0 ground electronic states involve a bending of the azido ligand. With the N_3 ligand still coordinated to the metal but in a cyclic geometry, Fe–N(N)N, it is crucial to what extent the vibrational motions of the nitrogens are coupled to those of the iron atom. In the case of a perfect decoupling and charge distribution in the ligand that is similar to the cyclic N_3 isomer, we would expect the azido ligand to be only weakly IR active for symmetry reasons just like in the case of the isolated C_{2v}-symmetrical azide radical. A time-resolved infrared detection of the N_3 ligand vibrations in the $D_{2,3}$ excited electronic configuration is then as difficult as the IR detection of a fully cleaved azide fragment in its cyclic $^2B_1$ state.

A conceivable intermediate in the photochemical reactions of parent complex **1** is thus a cyclic N_3 moiety coordinated to the iron center. In our DFT calculations (B3LYP/def2-TZVP)

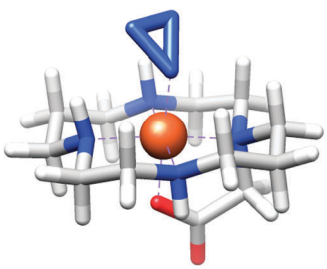

Fig. 10 DFT (B3LYP/def2-TZVP) structure of a possible intermediate in the photochemical Fe–N bond cleavage (orange: iron; blue: nitrogen; red: oxygen; grey: carbon; white: hydrogen).

we have indeed been able to locate such a minimum structure, as shown in Fig. 10.

The doublet state of this intermediate was calculated to be 9 kcal mol^{-1} more stable than the quartet state and 11 kcal mol^{-1} more stable than the sextet state, respectively. A cyclic coordination of N_3 to the iron complex is 56 kcal mol^{-1} higher in energy than the parent complex **1**, corresponding to 22 700 cm^{-1} of excess energy per molecule. With a 267 nm photon inducing the photolysis, the total excess energy delivered by the pump–pulse is 37 500 cm^{-1} per molecule. Similar results were obtained from our CASSCF(7,7) and NEVPT2 computations, where the cyclic intermediate was calculated to be 43 kcal mol^{-1} or 61 kcal mol^{-1} higher in energy, respectively. Hence, the structure shown in Fig. 10 containing a cyclic azido ligand might indeed be accessible in our photochemical reaction. Its mode analysis is fully consistent with the above intuitive notion: the highest frequency mode that is localized on the azide ligand is the cyclic-N_3 symmetric stretching (or breathing) vibration and is predicted to appear at 1779 cm^{-1}, *i.e.* in between the two characteristic vibrational resonances of the parent complex (*cf.* Fig. 2). Its transition dipole is calculated to be a factor of $\sim$200 smaller than that of the acetato-CO-stretching vibration of the cyclam ligand.

To follow up on this intriguing aspect of the primary photo-induced dynamics we are planning to perform experiments on compound **1** whose azido ligand is ^{15}N-isotopically labeled. Furthermore, we are currently setting up a time-resolved Raman-detection scheme to facilitate an unambiguous distinction between the linear and the cyclic forms of the azide fragment through their low-frequency vibrations. Finally, we will soon report on the dependence of the photo-induced ultrafast dynamics of this fascinating iron-azido complex on the photolysis wavelength.

IV. Conclusions

In summary, we have measured the elementary photo-physical and photo-chemical processes of **1** following its ultrafast electronic excitation with a femtosecond 266 nm light pulse. From previous steady-state studies a photo-reduction of the metal center was expected at an excitation wavelength of 266 nm. This expectation could be confirmed directly through a transient detection of the nascent azide radical at a sub-100 ps time scale. Taking geminate and non-geminate recombination reactions into account, the photolytic quantum yield was found to be $<$20%, *i.e.* surprisingly small. About one half of the initially excited complexes return to the electronic ground state presumably *via* internal conversion while the other half goes on to homolytically dissociate. The fragments efficiently recombine geminately at a time scale of $\sim$20 ps. As a result, the pronounced spectro-temporal evolution seen in the acetato-CO and azido stretching spectral regions on a time scale of several tens of picoseconds is governed by non-reactive vibrational energy relaxation as well as by recombinative ground-state recovery. We very much hope that these results will inspire further theoretical and experimental efforts in quantitatively understanding the primary photo-dynamics of model complexes serving as precursors to metal centers with unusually high oxidation states.

Acknowledgements

Financial support by the Deutsche Forschungsgemeinschaft through the Collaborative Research Center, SFB 813 "Chemistry at Spin Centers", is gratefully acknowledged.

References

1 M. Costas, M. P. Mehn, M. P. Jensen and L. Que Jr., *Chem. Rev.*, 2004, **104**, 939–986.
2 B. J. Wallar and J. D. Lipscomb, *Chem. Rev.*, 1996, **96**, 2625–2658.
3 M. Sono, M. P. Roach, E. D. Coulter and J. H. Dawson, *Chem. Rev.*, 1996, **96**, 2841–2887.
4 M. Costas, K. Chen and L. Que Jr., *Coord. Chem. Rev.*, 2000, **200**, 517–544.
5 S. G. Sligar, I. G. Denisov, T. M. Makris and I. Schlichting, *Chem. Rev.*, 2005, **105**, 2253–2277.
6 J. T. Groves and G. A. McClusky, *J. Am. Chem. Soc.*, 1976, **98**, 859–861.
7 D. Kumar, H. Hirao, L. Que Jr. and S. Shaik, *J. Am. Chem. Soc.*, 2005, **127**, 8026–8027.
8 S. Shaik, D. Kumar, S. P. de Visser, A. Altun and W. Thiel, *Chem. Rev.*, 2005, **105**, 2279–2328.
9 E. I. Solomon, T. C. Brunold, M. I. Davis, J. N. Kemsley, S. K. Lee, N. Lehnert, F. Neese, A. J. Skulan, Y. S. Yang and J. Zhou, *Chem. Rev.*, 2000, **100**, 235–349.
10 J. T. Groves, T. Takahashi and W. M. Butler, *Inorg. Chem.*, 1983, **22**, 884–887.
11 C. L. Hill and F. J. Hollander, *J. Am. Chem. Soc.*, 1982, **104**, 7318–7319.
12 W. D. Wagner and K. Nakamoto, *J. Am. Chem. Soc.*, 1989, **111**, 1590–1598.
13 J. F. Berry, E. Bill, E. Bothe, T. Weyhermüller and K. Wieghardt, *J. Am. Chem. Soc.*, 2005, **127**, 11550–11551.
14 C. A. Grapperhaus, B. Mienert, E. Bill, T. Weyhermüller and K. Wieghardt, *Inorg. Chem.*, 2000, **39**, 5306–5317.
15 K. Meyer, E. Bill, B. Mienert, T. Weyhermüller and K. Wieghardt, *J. Am. Chem. Soc.*, 1999, **121**, 4859–4876.
16 J. F. Berry, E. Bill, E. Bothe, S. DeBeer George, B. Mienert, F. Neese and K. Wieghardt, *Science*, 2006, **312**, 1937–1941.
17 N. Aliaga-Alcalde, S. DeBeer George, B. Mienert, E. Bill, K. Wieghardt and F. Neese, *Angew. Chem., Int. Ed.*, 2005, **117**, 2968–2972.
18 J. Torres-Alacan, O. Krahe, A. C. Filippou, F. Neese, D. Schwarzer and P. Vöhringer, *Chem.–Eur. J.*, 2011, DOI: 10.1002/chem.201103294.
19 F. Neese, Bonn University, **2011**.
20 C. T. Lee, W. T. Yang and R. G. Parr, *Phys. Rev. B: Condens. Matter*, 1988, **37**, 785–789.
21 A. D. Becke, *J. Chem. Phys.*, 1993, **98**, 5648–5652.
22 F. Neese, F. Wennmohs, A. Hansen and U. Becker, *Chem. Phys.*, 2009, **356**, 98–109.
23 A. Schafer, H. Horn and R. Ahlrichs, *J. Chem. Phys.*, 1992, **97**, 2571–2577.
24 F. Weigend and R. Ahlrichs, *Phys. Chem. Chem. Phys.*, 2005, **7**, 3297–3305.
25 A. P. Scott and L. Radom, *J. Phys. Chem.*, 1996, **100**, 16502–16513.
26 A. Klamt and G. Schuurmann, *J. Chem. Soc., Perkin Trans. 2*, 1993, 799–805.
27 A. Klamt, *J. Phys. Chem.*, 1995, **99**, 2224–2235.
28 B. A. Thrush, *Proc. R. Soc. London, Ser. A*, 1956, **235**, 143–147.
29 A. Treinin and E. Hayon, *J. Chem. Phys.*, 1969, **50**, 538–539.
30 C. R. Brazier, P. F. Bernath, J. B. Burkholder and C. J. Howard, *J. Chem. Phys.*, 1988, **89**, 1762–1767.
31 R. Tian, J. C. Facelli and J. Michl, *J. Phys. Chem.*, 1988, **92**, 4073–4079.
32 M. Bittererova, H. Ostmark and T. Brinck, *J. Chem. Phys.*, 2002, **116**, 9740–9748.
33 P. Zhang, K. Morokuma and A. M. Wodtke, *J. Chem. Phys.*, 2005, **122**, 014106.
34 J. Wasilewski, *J. Chem. Phys.*, 1996, **105**, 10969–10982.
35 P. C. Samartzis and A. M. Wodtke, *Phys. Chem. Chem. Phys.*, 2007, **9**, 3054–3066.

